AMERICAN SOCIETY FOR MICROBIOLOGY | Journal of Bacteriology®

RESEARCH ARTICLE

Hybrid Histidine Kinase BinK Represses *Vibrio fischeri* Biofilm Signaling at Multiple Developmental Stages

Denise A. Ludvik,[a,b] Katherine M. Bultman,[a,c] Mark J. Mandel[a,c]

[a]Department of Medical Microbiology and Immunology, University of Wisconsin—Madison, Madison, Wisconsin, USA
[b]Department of Microbiology-Immunology, Northwestern University Feinberg School of Medicine, Chicago, Illinois, USA
[c]Microbiology Doctoral Training Program, University of Wisconsin—Madison, Madison, Wisconsin, USA

ABSTRACT The symbiosis between the Hawaiian bobtail squid, *Euprymna scolopes*, and its exclusive light organ symbiont, *Vibrio fischeri*, provides a natural system in which to study host-microbe specificity and gene regulation during the establishment of a mutually beneficial symbiosis. Colonization of the host relies on bacterial biofilm-like aggregation in the squid mucus field. Symbiotic biofilm formation is controlled by a two-component signaling (TCS) system consisting of regulators RscS-SypF-SypG, which together direct transcription of the symbiosis polysaccharide Syp. TCS systems are broadly important for bacteria to sense environmental cues and then direct changes in behavior. Previously, we identified the hybrid histidine kinase BinK as a strong negative regulator of *V. fischeri* biofilm regulation, and here we further explore the function of BinK. To inhibit biofilm formation, BinK requires the predicted phosphorylation sites in both the histidine kinase (H362) and receiver (D794) domains. Furthermore, we show that RscS is not essential for host colonization when *binK* is deleted from strain ES114, and imaging of aggregate size revealed no benefit to the presence of RscS in a background lacking BinK. Strains lacking RscS still suffered in competition. Finally, we show that BinK functions to inhibit biofilm gene expression in the light organ crypts, providing evidence for biofilm gene regulation at later stages of host colonization. Overall, this study provides direct evidence for opposing activities of RscS and BinK and yields novel insights into biofilm regulation during the maturation of a beneficial symbiosis.

IMPORTANCE Bacteria are often in a biofilm state, and transitions between planktonic and biofilm lifestyles are important for pathogenic, beneficial, and environmental microbes. The critical nature of biofilm formation during *Vibrio fischeri* colonization of the Hawaiian bobtail squid light organ provides an opportunity to study development of this process *in vivo* using a combination of genetic and imaging approaches. The current work refines the signaling circuitry of the biofilm pathway in *V. fischeri*, provides evidence that biofilm regulatory changes occur in the host, and identifies BinK as one of the regulators of that process. This study provides information about how bacteria regulate biofilm gene expression in an intact animal host.

KEYWORDS biofilms, phosphorelay, two-component systems, symbiosis, *Vibrio fischeri*, *Aliivibrio fischeri*, biofilm

Animals are hosts to microbial partners that perform essential functions, including promotion of tissue and immune development, nutrient acquisition, and defense (1, 2). In many cases, the hosts emerge aposymbiotic (i.e., lacking their symbiont) and must then recruit and retain the correct symbiotic microbes from the environment. On the microbial side, these horizontally acquired symbionts often navigate multiple lifestyles, including a free-living environmental stage and a distinct host-associated phase (3). To understand how reproducible symbiotic colonization occurs against this

Citation Ludvik DA, Bultman KM, Mandel MJ. 2021. Hybrid histidine kinase BinK represses *Vibrio fischeri* biofilm signaling at multiple developmental stages. J Bacteriol 203:e00155-21. https://doi.org/10.1128/JB.00155-21.

Editor George O'Toole, Geisel School of Medicine at Dartmouth

Address correspondence to Mark J. Mandel, mmandel@wisc.edu.

Received 26 March 2021
Accepted 13 May 2021
Accepted manuscript posted online 24 May 2021
Published

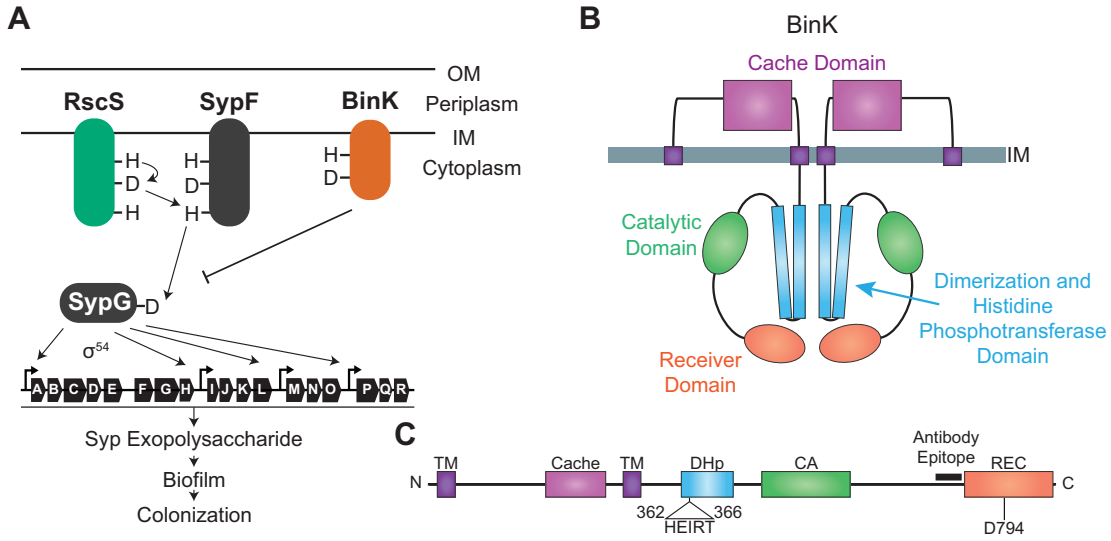

FIG 1 BinK signaling and domain organization. (A) Model of the biofilm pathway in strain ES114 relevant to this study. RscS signals through SypF to SypG, which is a σ^{54}-dependent transcriptional activator of the *syp* locus. Expression of the *syp* locus is required for biofilm formation. BinK inhibits biofilm production and feeds into the pathway at an unknown location at or above SypG. (OM, outer membrane; IM, inner membrane). (B) Putative subcellular localization of a BinK homodimer. (C) BinK domain diagram. Positions of key residues and the epitope used to generate the BinK peptide antibody (722 to 742) are annotated. TM, predicted transmembrane domains.

backdrop of distinct microbial life stages, we can use a model system in which a host organ is colonized by only a single bacterial partner. Here, we focus on marine *Vibrio fischeri* bacteria and their colonization of the light organ of the Hawaiian bobtail squid, *Euprymna scolopes* (4, 5). *V. fischeri* gains exclusive access to the squid's light organ niche and creates luminescence that the squid manipulates as a counterillumination camouflage strategy (6, 7). Within hours of the aposymbiotic squid hatching, *V. fischeri* bacteria colonize the light organ (8, 9). In addition to the binary nature of the symbiosis and the ability to rear both partners separately, the amenability of *V. fischeri* to sophisticated genetic manipulation and the power to image at the direct site of infection provide a powerful tool box to study how genes and their products influence bacterial colonization.

Biofilm formation by the symbiotic bacteria is fundamental to the colonization of the squid host (3, 10–15). During the establishment of the symbiosis, squid recruit *V. fischeri* by pumping seawater through the mantle cavity and over the light organ. Biofilm formation is required for *V. fischeri* to aggregate in the host mucus, and *V. fischeri* mutants unable to synthesize biofilm are unable to colonize the squid (10, 11). The polysaccharide component of the biofilm is the symbiosis polysaccharide (Syp), whose production is encoded by the 18-gene *syp* locus on the *V. fischeri* second chromosome (11). Expression of this locus is controlled by a two-component phosphorelay (Fig. 1A). In strain ES114, the current model posits that the hybrid sensor kinase RscS autophosphorylates at residue H412 in its dimerization and histidine phosphotransferase (DHp) domain and then relays the phosphoryl group to D709 in its receiver domain (REC) (16). The phosphoryl group is then relayed to residue H705 in the histidine phosphotransfer (HPt) domain of a distinct hybrid sensor kinase, SypF (17, 18). SypF then phosphorylates D53 in the REC domain of response regulator SypG (17, 19). Phospho-SypG acts as a σ^{54}-dependent enhancer binding protein to promote transcription of the *syp* locus (11, 20). SypF has additional effects, including regulation of the activity of serine kinase/phosphatase SypE to inactivate/activate its target, SypA, which influences Syp biofilm formation downstream of *syp* transcription (21).

Previously, we identified the biofilm regulator BinK as a strong inhibitor of symbiotic biofilm formation (22). BinK was identified in an insertion sequencing screen in which a mutant library of *V. fischeri* was analyzed before and after colonization of squid hatchlings

to find genes that influenced colonization (23). Mutants of *binK* were overrepresented in the output pool compared to the input, suggesting that deletion of *binK* confers an advantage during the colonization process. Upon further study, it was determined that deletion of *binK* confers a competitive advantage against the wild-type (WT) strain during squid colonization, and the mutant forms larger aggregates on the surface of the squid light organ (22). Overexpressing BinK leads to a substantial reduction in symbiotic biofilm formation and prohibits bacteria from colonizing the host. BinK, which is conserved across *V. fischeri* strains (15), was also identified to be an important colonization regulator in a squid colonization experimental evolution study (14). Natural *V. fischeri* fish and seawater isolates that were experimentally evolved to colonize squid were able to do so as a result of spontaneous mutations in *binK* (14). Strain ES114 does not form robust biofilms outside the squid. However, we can use culture-based assays with an RscS-overexpressing allele (termed *rscS**) that approximates *in vivo* biofilm phenotypes to study BinK function, and with those approaches we demonstrated that deletion of *binK* can lead to wrinkled colony formation, higher transcription of the *syp* locus, and higher production of the Syp exopolysaccharide (22). Overexpression of *sypG* is epistatic to inhibitory signaling from overexpression of *binK* (22). The Δ*binK* strain is significantly derepressed for biofilm formation, and in that background, calcium stimulates colony biofilm formation without the need for induction by *rscS** alleles (24). The calcium induction system led to the discovery of biofilm regulator HahK, which influences biofilm development in response to host nitric oxide (24, 25).

Given the prominence of BinK as a strong negative regulator of biofilms across various *V. fischeri* natural isolates, here we pursued multiple questions regarding its function during symbiosis. First, while BinK has the predicted structure of a hybrid histidine kinase, we asked whether it requires its putative phosphorylation sites for function. Second, given the strong phenotypes of BinK, we asked whether canonical squid isolate ES114 would be capable of colonizing squid in the absence of the positive regulator RscS if the negative regulator BinK was also removed. We found that RscS was dispensable for colonization in the absence of BinK, and this result enabled us to investigate the relative role of each protein during symbiotic colonization. Third, using direct imaging of a fluorescent *syp* transcriptional reporter, we asked whether symbiosis polysaccharide gene expression is regulated in the host by comparing regulation at two distinct time points (and therefore distinct sites with the host) and by comparing both wild-type and various mutant strains. Overall, this work provides an intriguing look into how biofilm signaling is regulated when a symbiotic microbe encounters its animal host.

RESULTS

BinK requires its conserved two-component histidine and aspartate residues for function. We identified BinK as an orphan hybrid histidine kinase that inhibits biofilm formation and is a negative regulator of squid colonization (22). Protein domain prediction indicated that BinK has the conserved dimerization and histidine phosphotransferase (DHp) domain and catalytic (CA) domain typical of a two-component sensor kinase, and it also contains an additional receiver (REC) domain making it a hybrid sensor kinase (Fig. 1B) (26–29). His362 in the DHp domain and Asp794 in the REC domain are the predicted sites for phosphorylation in BinK (Fig. 1C) (22). Phosphotransfer through such sites is typically required for signaling by sensor kinases, but there are examples where this is not the case (17, 30, 31). Therefore, we first asked whether His362 and Asp794 are necessary for BinK function.

To assess the function of individual alleles, we conducted colony biofilm assays. We started with a Δ*binK* strain and then introduced the *binK* gene (including 300 bp of upstream and downstream sequence) into the neutral chromosomal *att*Tn*7* site (Fig. 2A). This approach enabled us to test the wild-type and mutant alleles in comparable isogenic backgrounds. The strain background also has an allele to induce biofilm formation under culture conditions through the overexpression of RscS. This allele, termed *rscS**, is carried on the chromosome at the native *rscS* locus (Fig. 2A) (32). In this background, deletion of *binK* results in a wrinkled colony morphology when the strain is grown at 28°C,

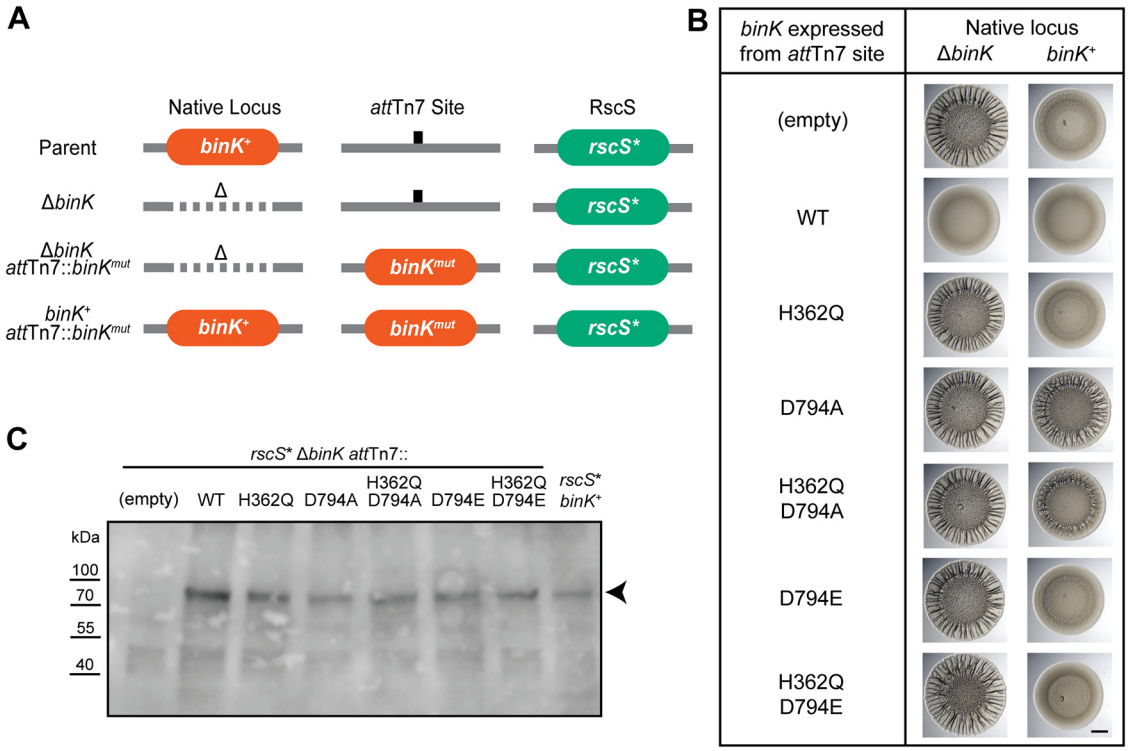

FIG 2 BinK requires H362 and D794 to inhibit colony biofilms. (A) Genome representations of the different strains used to assess *binK* alleles. The parent ES114 *rscS** strain (MJM1198) was used to induce biofilm formation for wrinkled colony assays on plates. The *att*Tn*7* site is located on chromosome I and the native locus of *binK* is on chromosome II. *mut* designates a mutant allele of *binK*, while Δ indicates a clean deletion at that locus. (B) Wrinkled colony assay of the strains indicated, grown at 28°C for 48 h. Mutations (or wild-type [WT] control) expressed at the *att*Tn*7* site are listed beside each spot. In the left column, the expressed allele is the only *binK* allele in the cell, while in the right column, wild-type *binK* is additionally present at its native locus. Bar is 2 mm. (C) Western blot of whole-cell lysates assessed with a peptide antibody against BinK. Arrow indicates BinK, which is predicted to be 97 kDa (61) and which is absent in the strain that does not encode the protein.

whereas a strain with a functional *binK* has a smooth colony morphology (22). To test whether the His362 and/or Asp794 are required for BinK function, we constructed H362Q and D794A mutants, which have been shown to mimic the unphosphorylated state when similarly introduced into homologous domains (16, 33). In an otherwise Δ*binK* background, alteration of either individual residue or of both residues in the same protein resulted in a nonfunctional BinK (Fig. 2B). We next asked whether a predicted phosphomimetic allele of the REC domain D794E is functional. This allele was constructed and was unable to complement the lack of BinK in the *rscS** biofilm induction model (Fig. 2B). Using Western blot analysis with a polyclonal antibody raised against a BinK cytoplasmic epitope, we demonstrated that the mutant proteins are expressed (Fig. 2C). Together, these results provide genetic evidence that phosphorylation of BinK residues is required for its function. Given that we did not observe complementation with either the D794A, which is predicted to be nonphosphorylatable, or with the putative phosphomimetic D794E allele, we expect that phosphoryl groups at this residue are transferred to (or from) a downstream signaling partner and that this signaling is required for BinK to inhibit biofilm formation.

BinK merodiploid analysis reveals a dominant negative phenotype for the D794A allele. Our data above demonstrated that the H362Q and D794A alleles were individually nonfunctional. Given that histidine kinases typically operate as homodimers, we next inquired whether the BinK(H362Q) or BinK(D794A) alleles had any effect when expressed in a cell that also expressed wild-type BinK protein. We continued to express the test alleles from the *att*Tn*7* site, but now did so in a strain expressing wild-type *binK* from the native locus. In the wrinkled colony assay, the nonfunctional H362Q allele was recessive to the wild-type allele, as expected, but the

D794A allele exhibited a dominant negative phenotype, displaying a lack of biofilm inhibition even in the presence of the wild-type allele (Fig. 2B). A similar dominance was observed for the D794A allele, even if the H362Q allele was introduced on the same polypeptide, expressed from the *att*Tn*7* site (Fig. 2B). While either the H362Q or the D794A alteration disables BinK's biofilm inhibitory function, the latter allele additionally interferes with the ability of a wild-type copy of BinK to inhibit biofilm formation.

Our data described above demonstrated that the putative phosphomimetic D794E allele of BinK was similarly nonfunctional, like the D794A allele, when expressed as the only BinK allele in the cell. Merodiploid analysis revealed, however, that the D794E allele did not interfere with BinK activity in *trans* (Fig. 2B). This was the case whether it was the only alteration in *binK* or was in the context of a double *binK*(H362Q, D794E) allele (Fig. 2B). Therefore, inactivation of the REC domain does not correlate directly with the dominant interfering phenotype. However, it may be the case that an unphosphorylated D794 (and the D794A allele that cannot be phosphorylated) leads to inhibition of BinK activity, whereas phosphorylated D794 (mimicked by the D794E allele) does not.

Sensor kinases can perform both phosphatase and kinase activities (34). To ask whether BinK kinase or phosphatase activity is used for biofilm inhibition, we changed individual residues in the DHp domain that are predicted to differentially affect kinase versus phosphatase activities of the protein. BinK contains a conserved EXXT motif immediately after the conserved His362 residue (Fig. 1C). This region of the H-box (i.e., the conserved phosphoryl group binding His and surrounding region) is important for coordinating the phosphotransfer reactions in two-component proteins (35). In BinK we constructed E363A, T366Q, and T366A alleles that are predicted to eliminate kinase activity, reduce phosphatase activity, and eliminate phosphatase activity (with possible effects on autokinase activity), respectively (35–41). Colony biofilm assays revealed nonfunctional BinK in each case (see Fig. S1 in the supplemental material). This result further supports a role for phosphotransfer through BinK in its functional role.

Single-copy phosphomimetic SypG is epistatic to BinK overexpression. As an orphan histidine kinase, BinK has no known paired response regulator. In a previous study, we demonstrated that a separate RscS-dependent pathway that relies on signaling through SypE was insensitive to BinK activity (22). Therefore, we can proceed to study BinK signaling architecture in an Δ*sypE sypF2* mutant background to isolate the core biofilm phosphorelay. Note that in this strain background, wrinkled colony formation is observed upon overexpression of SypG (without the requirement for *rscS**) (18, 42). In our previous study, we demonstrated that overexpression of SypG led the cell to be insensitive to overexpression of BinK in a wrinkled colony assay (22). This result suggested that SypG was epistatic to BinK. To further probe the genetic relationship between BinK and SypG, we constructed a phosphomimetic SypG allele at the native *sypG* locus. Hussa et al. demonstrated that a plasmid containing the SypG(D53E) allele conferred increased *syp* transcription and wrinkled colony formation in a Δ*sypE sypF2* strain (18). We introduced the same amino acid change into chromosomal *sypG* within the Δ*sypE sypF2* genetic background. We proceeded to determine that overexpression of BinK does not reduce the colony biofilm produced in the Δ*sypE sypF2 sypG*(D53E) background (see Fig. S2 in the supplemental material). Therefore, this experiment supports and extends our previous work and provides strong evidence that BinK acts upstream of SypG in the control of *syp* transcription and biofilm development. We then proceeded to examine the relative impacts of RscS and BinK on colonization phenotypes *in vivo*.

RscS is not required for aggregation or squid colonization in a strain lacking BinK. In strain ES114, the positive regulator RscS and the negative regulator BinK both exert strong impacts on colonization, and both act through the response regulator SypG. We therefore considered models in which RscS and BinK exert opposing influence on *syp* gene transcription during squid colonization. Deletion of *rscS* alone leads to severe *in vivo* biofilm and colonization defects, whereas deletion of *binK* alone leads to enhanced biofilm production and improved colonization in a competitive assay (10, 22, 43). Given these

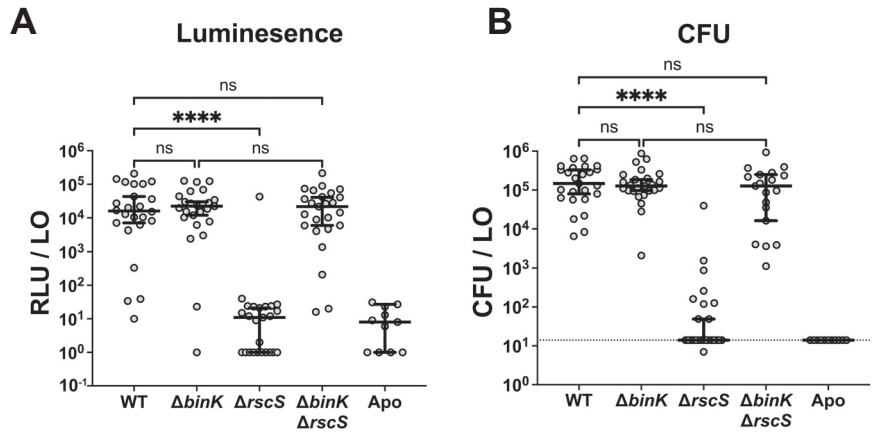

FIG 3 RscS is not required for squid colonization in a strain lacking BinK. Bacteria were inoculated into filter-sterilized Instant Ocean (FSIO) containing squid and allowed to colonize for 3 h. Squid were washed and then maintained for 2 days to allow establishment of the symbiosis. Shown are data on the luminescence (relative light units [RLU]) (A) and CFU (B) per light organ (LO) at 48 h postinfection (hpi). Each dot represents an individual animal. The dashed line indicates the limit of detection for CFU/LO. Apo, aposymbiotic. For both graphs, data are pooled from three replicate experiments. Bars represent the median for each strain with a 95% confidence interval. Statistical significance was calculated using Kruskal-Wallis test with Dunn's multiple-comparison tests. ns, not significant; ****, $P < 0.0001$.

opposing phenotypes, we asked whether removal of both regulators—RscS and BinK—would enable the bacteria to colonize the host. An examination of experiments in diverse *V. fischeri* strains provides some insight into this question. Strains can improve their ability to colonize squid in the laboratory by mutation of *binK*, and this includes strain MJ11, which naturally lacks RscS (14, 22). The same MJ11 strain can colonize squid robustly if RscS from squid symbiont ES114 is introduced (13). Together, these results support our model that RscS and BinK could exhibit opposing activities, but we remained uncertain as to what we would observe in native squid symbiont ES114. If RscS is mainly required to counteract the negative regulation of BinK, then elimination of both regulators should allow the bacteria to colonize the squid host. However, if RscS is required to transduce a specific signal from the host, then we predict that elimination of both regulators would not allow for colonization.

To test these models, we conducted single-strain colonization assays. As has been shown previously, an Δ*rscS* mutant exhibits a significant colonization defect (Fig. 3) (43). The Δ*binK* mutant is known to exhibit a competitive advantage over the wild type (22), yet in single-strain colonization displays similar bacterial yields and luminescence (Fig. 3). The Δ*binK* Δ*rscS* double mutant strain was able to colonize up to levels indistinguishable from those of the wild-type strain (Fig. 3). This result therefore supports the model that in ES114 BinK and RscS each antagonize the other's activity, and that in the absence of the negative regulator BinK, the positive regulator RscS is no longer required for single-strain colonization.

The above result was surprising in that we identified a condition under which RscS, discovered 20 years ago as a strong colonization factor (43), was no longer required for squid colonization in strain ES114. This prompted us to ask whether the key symbiotic behavior regulated by RscS—*in vivo* aggregate formation—occurs in the Δ*binK* Δ*rscS* background. For this experiment, we introduced a plasmid that constitutively expresses green fluorescent protein (GFP) into the colonizing strains from Fig. 3, and we asked whether these strains form biofilm aggregates in the squid mucus field. Direct visualization of the bacterial cells revealed the presence of biofilm aggregates in the host for the Δ*binK* Δ*rscS* cells (Fig. 4A). Notably, the size of these aggregates was comparable to that of those formed by Δ*binK* single mutant cells, which were larger than the aggregates formed by wild-type *V. fischeri* (Fig. 4A and B). This result therefore

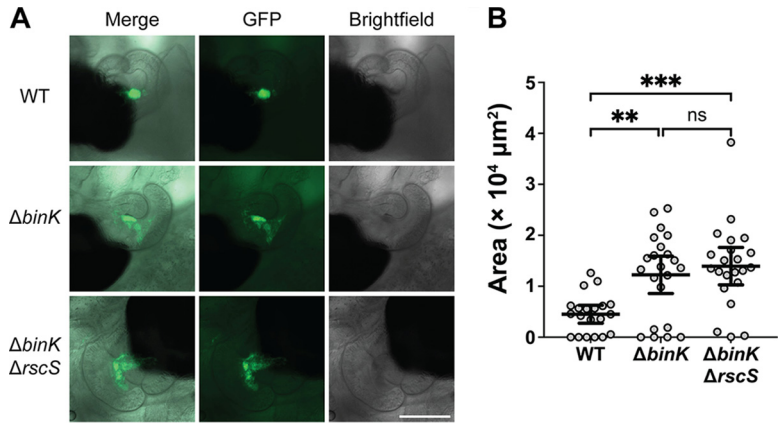

FIG 4 RscS does not impact aggregation in a strain lacking BinK. Imaging of bacterial aggregates in host mucus using fluorescence microscopy with the Zeiss Axio Zoom fluorescence microscope. Squid were inoculated with *V. fischeri* cells that constitutively express green fluorescent protein (GFP) from the pVSV102 plasmid and imaged at 3 to 4 hpi. (A) Representative images of aggregates of approximately median size for each strain. Bar, 200 μm, with all panels at the same scale. (B) Quantification of aggregate area. Each dot represents one aggregate. A measure of zero indicates that no aggregate was present. Significance was determined with a Kruskal-Wallis test and Dunn's multiple-comparison tests (ns, not significant; **, $P < 0.01$; ***, $P < 0.001$). The median area with a 95% confidence interval is displayed for each group. The data are pooled from two replicate experiments. WT, wild-type ES114 (MJM1100).

reveals that RscS is not required for aggregate formation in a background lacking BinK, and RscS does not contribute to aggregate size in this background.

The above results prompted us to ask whether RscS performs any detectable function in a strain lacking BinK. We employed a sensitive competition assay to ask whether strains lacking RscS exhibit a defect upon coinoculation. In a competitive colonization assay in which the Δ*binK* Δ*rscS* strain was coinoculated with a LacZ-expressing Δ*binK* single mutant, the strain lacking RscS exhibited an approximately 100-fold defect in the competition (Fig. 5).

In the absence of BinK, *syp* transcription *in vitro* does not require RscS. Recent work demonstrated that in a strain lacking BinK, RscS is not required for colony biofilm

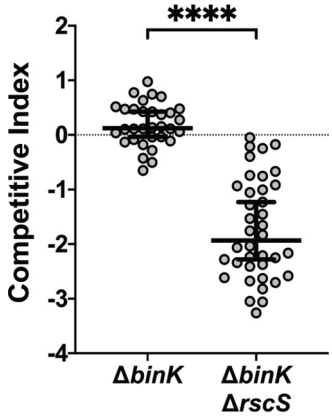

FIG 5 RscS is required for competitive fitness in a Δ*binK* background. Competitive fitness of the indicated strains (unlabeled) compared to that of a Δ*binK* strain (labeled with LacZ). Squid were exposed to a mixed inoculum of the two strains for 3 h, then assessed at 48 hpi. Blue versus white CFU counts on LBS–X-Gal were used to determine the representation of each strain in the competition. The competitive index is equal to the $\log_{10}$-transformed value of the ratio (indicated strain/Δ*binK* strain) after competition normalized to its ratio in the input inoculum. Each point represents the competitive index from an individual squid. The median ratio with a 95% confidence interval is represented by the bar. Statistical significance was calculated with a Mann-Whitney U test (****, $P < 0.0001$).

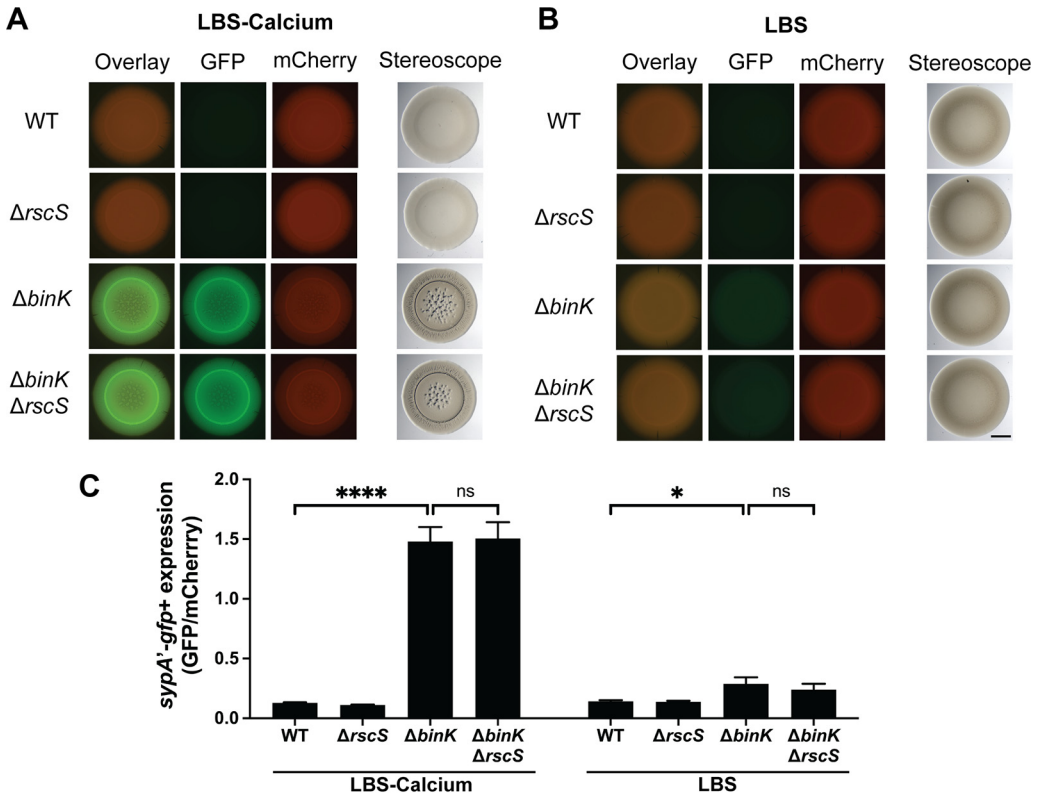

FIG 6 RscS does not alter *syp* production on agar in strains lacking BinK. *syp'-gfp*$^+$ transcriptional reporter activity normalized to constitutive mCherry from strains carrying pM1422. (A, B) Each strain was spotted onto LBS or LBS-calcium medium and grown for 48 h at 25°C. Images were taken on both a Zeiss Axio Zoom fluorescence microscope and Leica brightfield stereoscope. Bar, 2 mm; all images in panels A and B are at the same scale. (C) Quantification of the fluorescence intensity. GFP intensity of the entire colony was normalized to mCherry intensity. Each bar represents the average GFP/mCherry reading of five different colonies from replicate experiments on two distinct days. Error bars are standard deviations. Statistical significance was determined with a two-way analysis of variance (ANOVA) analyzing the effect of strain background and medium on fluorescence, with Tukey's test for multiple comparisons. ns, not significant; *, $P < 0.05$; ****, $P < 0.0001$.

formation when the symbiotic biofilm is induced with an additional 10 mM calcium in the medium (Luria-Bertani salt [LBS]-Ca) (24). We therefore examined a *sypA'-gfp*$^+$ transcriptional reporter for cells grown on LBS-Ca agar, in strains that lack BinK, RscS, or both regulators. We determined that GFP activity from the reporter is induced in the Δ*binK* background, and the presence or absence of *rscS* in this background did not impact *syp* expression (Fig. 6A and C). Similarly, the wrinkled colony biofilm phenotype was observed in both the Δ*binK* and Δ*binK* Δ*rscS* strains. Next, we examined the same reporter when the cells were grown on rich medium without the additional calcium (LBS). On LBS agar, the overall induction was lower than that on LBS-Ca, and strains did not wrinkle. However, we still detected induction of the reporter in the Δ*binK* strain compared to the WT parent. The induction is unaffected by the absence of *rscS* from this background (Fig. 6B and C). In summary, we can readily detect *syp* gene transcription in the Δ*binK* background when strains are grown on different solid media, and this induction is independent of RscS.

BinK represses *syp* transcription in the squid crypts. We next examined expression of the *sypA'-gfp*$^+$ transcriptional reporter in *V. fischeri* cells that had aggregated in the host mucus (3 to 4 h postinfection [hpi]). The results shown in Fig. 7A and C reveal indistinguishable overall levels of GFP activity in WT, Δ*binK*, and Δ*binK* Δ*rscS* cells in the aggregates of each animal examined. We note some limitations to these data. Given that cells spend a short period of time in the aggregate stage—on the order of 1 to 2 h—it is unclear whether the reporter is revealing the steady-state transcription

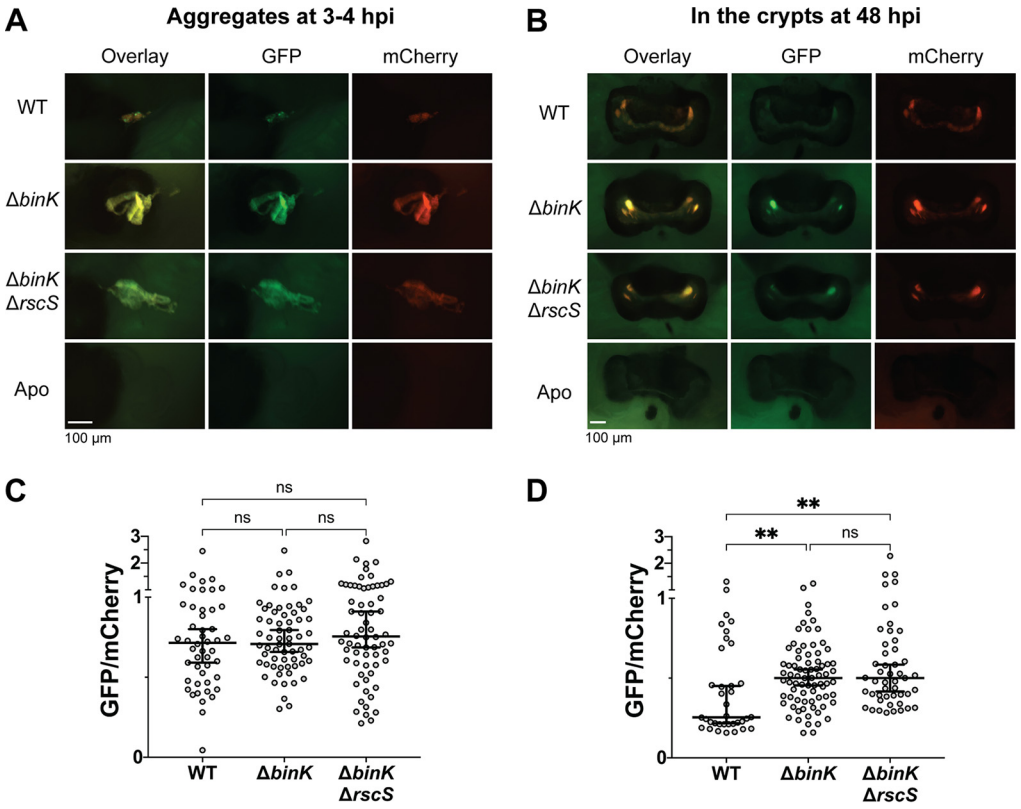

FIG 7 BinK inhibits *sypA* transcription in the crypts. Imaging of *V. fischeri* containing the pM1422 *sypA′-gfp*$^+$ reporter plasmid (that encodes constitutive mCherry) (A, C) while aggregating in host mucus at 3 to 4 hpi or (B, D) in host crypts at 48 hpi. For quantification (C, D), intensity of GFP and mCherry was measured for each individual aggregate or crypt, background signal was subtracted, and GFP was normalized to the mCherry level. Zen Blue software was used to collect signal and background measurements. Each dot represents an individual aggregate or crypt. Bars represent the median GFP/mCherry ratio with 95% confidence intervals. Statistical significance within each location was determined by a Kruskal-Wallis test with Dunn's multiple-comparison tests (ns, not significant; **, $P < 0.01$). Data for each bacterial location are pooled from at least 3 replicate experiments that each contained 4 to 8 squid per strain.

levels from the aggregate or whether this information integrates time prior to the aggregation stage (growth in liquid medium and in seawater). Nonetheless, we present these data for two reasons. First, any physiological response that uses transcription to regulate symbiosis would be subject to similar constraints. Second, the similarity of the data points provides a useful control for the data in the crypts that will be described below. Even with these caveats, we can conclude that the absence of RscS does not diminish the median level of *sypA* transcription in the Δ*binK* background. We note that there was more heterogeneous *sypA′-gfp*$^+$ activity across the aggregate in the wild type compared to that in samples that lacked BinK (Fig. 7A).

We proceeded to conduct a similar analysis of the transcriptional reporter in the light organ crypts (48 hpi). At this point, we observed a notable difference between the Δ*binK* strain and the wild type, with substantially elevated *sypA* transcription in the cells lacking BinK (Fig. 7B and D). The absence of RscS did not affect the *sypA* reporter. From this imaging, we conclude that a normal function of BinK is to repress *syp* transcription in the crypts.

DISCUSSION

By studying the *V. fischeri*-squid symbiosis model, we have refined our understanding of how bacterial biofilm signaling is regulated at the initiation of colonization. This study provides evidence that BinK acts as a hybrid histidine kinase, defines novel biofilm regulation in the host, describes a role for BinK in that regulation, and reveals that

the key ES114 colonization factor RscS is dispensable in the absence of BinK. These major conclusions are discussed in detail below.

BinK acts as a hybrid histidine kinase. In our previous study, we identified BinK as a putative hybrid histidine kinase based on its predicted domain structure containing CA, DHp, and REC domains (Fig. 1) (22). Furthermore, experimental evolution studies to improve squid colonization of other *V. fischeri* strains revealed spontaneous *binK* point mutations that altered its CA and HAMP domains, which approximated the phenotypes of Δ*binK* strains, suggesting key roles for these domains in BinK function (14). In this work, we used a combination of targeted mutants with a newly developed anti-BinK peptide antibody to demonstrate that mutagenesis of predicted phosphorylation sites creates BinK proteins that are nonfunctional.

In most cases, histidine kinases dimerize, and our results provide genetic support for the hypothesis that this occurs in the case of BinK. In particular, we found that a BinK protein containing a REC domain that is locked as nonphosphorylated with the D794A allele is not only nonfunctional, but is dominant negative, as it interferes with the signaling of a wild-type *BinK* allele expressed in the same cell. There are published cases in which one monomer's REC domain interacts with the same monomer's DHp domain (in *cis*) and other cases in which it interacts with the partner monomer's DHp domain (in *trans*) (44, 45). In both cases, however, dynamic movement of both monomers is required across the dimer interface (35, 46). It seems likely that the BinK D794A allele disrupts some aspect of this dynamic process that is still intact in heterodimers containing the phosphomimetic D794E allele. Therefore, BinK REC domain phosphorylation may both contribute to phosphoryl group flow and regulate the ability of BinK to interact in productive dimers.

Our data support a model in which phosphoryl groups flow from/to a downstream signaling partner through the BinK REC domain. The lack of complementation of a Δ*binK* allele with either the *binK*(D794A) or *binK*(D794E) alleles provide support for this model, in spite of differences in the merodiploid analysis described above. Additionally, the double *binK*(H362Q, D794E) allele is nonfunctional but not disruptive in the presence of a wild-type allele, suggesting that phosphoryl group flow can proceed in *cis* through a single BinK monomer even when present in mixed dimers with the double mutant. We note that there are examples in the literature where a REC domain regulates activity of the DHp domain and does not directly transfer phosphoryl groups (30, 31, 47). While this is possible for BinK, it seems unlikely given the genetic results here. Future biochemical analysis of BinK phosphotransfer will be necessary to further advance these studies. In particular, such analysis may enable asking whether BinK acts as a kinase or phosphatase when it inhibits biofilm formation. Without knowledge of the direct downstream partner of BinK, this question is difficult to address at present.

Considering that a phosphomimetic SypG is epistatic to BinK, it is likely that BinK is acting to control the phosphorylation of SypG. Our results indicate that the BinK His and Asp residues are necessary for activity. Thus, we predict BinK acts indirectly on SypG through the HPt domain in another regulator. Among known players, the HPt domain that has been shown to mediate phosphorylation of SypG is that of SypF (17, 24), making SypF a likely candidate. It is also possible that the relevant partner has yet to be identified. Genetic approaches to identify and characterize relevant partners will provide insight into the pathway downstream of BinK.

RscS is dispensable for colonization in strain ES114 lacking BinK. We found that in strain ES114, *rscS* is not required for squid colonization in a Δ*binK* background. Strains lacking both regulators colonize to a level comparable to that of the wild type, although we found through competitive colonization analysis that there still remains a role for RscS in this background (Fig. 3 and 5). There are three major phylogenetic groups of *V. fischeri* (15). Relevant for this work, the ancestral group C strains include Mediterranean squid symbionts such as strain SR5. These strains encode functional BinK but do not encode RscS, and it is unclear how they can colonize squid without the biofilm-promoting activity from RscS (15). Group C strains also include fish symbionts such as MJ11, which cannot colonize squid unless they gain RscS or lose BinK

(13, 14). Derived from this group is group B, which includes strain ES114, which is the focus of the present study. Squid symbionts in group B typically encode both RscS and BinK, and mutation of RscS leads to an inability to colonize the squid (13, 15). In this study, it was found that when *binK* is deleted, strain ES114 no longer requires *rscS* for colonization (Fig. 3). This result mirrors a previous finding in group C, namely, that strains lacking RscS (due to evolution) and also lacking BinK (due to directed mutation) could colonize squid (14). Given the diversity of biofilm regulation across *V. fischeri*, this result was not expected and highlights conserved aspects of regulation that are shared across much of the species (15). It therefore seems that one of the main functions of RscS is to antagonize BinK's negative regulation of biofilm; without the negative regulator, the positive regulator is no longer absolutely required for host colonization. From the evolutionary tree, we know that *binK*—which is found throughout the species—predates the horizontal gene transfer event that enabled acquisition of *rscS*, which is only present in a derived group of *V. fischeri* strains (13, 15). Therefore, our work raises the question of whether there are other factors that antagonize BinK activity in strains that colonize squid independent of RscS (e.g., the group C Mediterranean squid symbionts). It seems likely that such activity would be sufficient to enable colonization, given that mutations in *binK* facilitate colonization by strains that are otherwise unable to colonize well (14).

BinK is a key regulator across the symbiotic life cycle. In a previous study, we used a fluorescent biofilm gene promoter fusion to examine gene expression in liquid medium (22). In this work, we expanded on that approach to examine expression of *sypA′-gfp*$^+$ on solid medium and *in vivo* during colonization. On solid agar, we observed high levels of reporter expression under conditions known to induce Syp biofilm formation (LBS-calcium [24]). We observed a less dramatic yet significant induction on medium where the Syp biofilm is not visibly apparent (LBS), revealing the sensitivity of this reporter. Our results provide evidence for expression of the *syp* biofilm in the aggregates, when biofilm formation is known to be required for colonization. We also demonstrate that in the absence of BinK, there is expression of *syp* reporter in the crypts, which supports a role for BinK in repressing biofilm gene expression at this later stage in the wild-type strain. Building on our observation above that RscS is dispensable for colonization in strains lacking BinK, we observed similar levels of *syp* reporter expression in Δ*binK* and Δ*binK* Δ*rscS* strains. Our discovery that BinK functions to repress *syp* expression in the crypts hints that BinK regulation may serve a role in the daily expulsion of bacteria from squid at dawn. Little is known about how this process is regulated, yet it occurs daily in the mature symbiosis for the duration of the host's lifetime. If there is a role for BinK in the diel cycle, it may help to explain why *binK* genes are widely conserved in *V. fischeri* despite the mutant having a competitive advantage (14, 15, 22). It seems likely that while the absence of BinK is beneficial to enter the squid host, the absence of the regulator (and subsequent inappropriate biofilm formation at later stages) may be detrimental to the daily homeostasis that is maintained long-term in the squid. We also examined *sypA′-gfp*$^+$ reporter activity in biofilm aggregates. The average expression level within aggregates was similar for wild-type or Δ*binK* mutant cells, but we observed greater heterogeneity in the expression in wild-type cells. This suggests that in the presence of BinK, there is more variability in biofilm expression, and this is worthy of further study.

This work provides an exciting view into how biofilm gene expression is regulated *in vivo*. We know that within a few hours, planktonic bacteria transition to a biofilm state in the host mucus (3, 48). Despite a number of biofilm regulators being identified, how this process is controlled at the host interface is not well understood. Our results provide evidence that this regulation is dynamic over the course of colonization, as evidenced by the BinK-dependent repression that occurs specifically in the crypts at 48 hpi but is not evident in the aggregates at 3 to 4 hpi. We propose that the interaction of BinK with host-derived compounds may lead to downregulation of biofilm genes as bacteria transition from the biofilm aggregates during initiation to cells in the crypts

during the persistence stage. Finally, we observed similar sizes of *in vivo* biofilm aggregates in the host in Δ*binK* and Δ*binK* Δ*rscS* strains, arguing that there is no requirement for stimulation of biofilm through RscS to initiate a productive symbiosis. We therefore posit that a key regulatory mechanism to control the planktonic-to-biofilm transition is host inhibition of BinK.

In summary, this work provides novel insight into the function of hybrid histidine kinase BinK, its relationship to RscS is regulating symbiotic biofilm formation, and the temporal control of symbiotic biofilm gene expression. Future work will continue to examine the signaling architecture downstream of BinK and host-derived molecules that may regulate BinK activity.

MATERIALS AND METHODS

Bacterial strains, plasmids, and media. *V. fischeri* and *Escherichia coli* strains used in this study are listed in Table 1. Plasmids used in this study are listed in Table 2. *V. fischeri* strains were grown at 25°C or 28°C in Luria-Bertani salt (LBS) medium (25 g Difco LB broth [BD], 10 g NaCl, and 50 ml 1 M Tris buffer [pH 7.5], per liter). *E. coli* strains, used for cloning and conjugation, were grown with shaking at 37°C in Luria-Bertani (LB) medium (25 g Difco LB broth [BD] per liter). Growth media were solidified with 1.5% agar (15 g Bacto agar [BD] per liter) as needed. When necessary, antibiotics were added to the medium at the following concentrations: erythromycin (Erm), 5 μg/ml for *V. fischeri*; kanamycin (Kan), 100 μg/ml for *V. fischeri* and 50 μg/ml for *E. coli*; and chloramphenicol (Cam), 5 μg/ml for *V. fischeri* and 25 μg/ml for *E. coli*. The *E. coli* strain π3813 containing pKV496 is a thymidine auxotroph and was grown in LB with 50 μg/ml kanamycin supplemented with 0.3 mM thymidine (49, 50).

DNA synthesis and sequencing. Each of the primers listed in Table 3 was synthesized by Integrated DNA Technologies (Coralville, IA). Full inserts from all cloned constructs were verified by Sanger DNA sequencing at Northwestern University Feinberg School of Medicine Center for Genetic Medicine, Functional Biosciences via UW—Madison, or the UW—Madison Biotechnology Center. Sequence data were analyzed with SeqMan Pro (DNAStar software) and Benchling. For cloning and sequencing PCRs, we used Q5 high-fidelity DNA polymerase (NEB). For diagnostic PCR, we used GoTaq polymerase (Promega).

Construction of *att*Tn*7*::*binK* mutant alleles. The previously generated pTn*7*-*binK* plasmid, which uses a mini-Tn*7* delivery vector backbone (pEVS107), was purified and used as a template. Point mutations to the *binK* sequence on the plasmid were designed using the NEBaseChanger tool and constructed with the Q5 site-directed mutagenesis kit (New England BioLabs, Inc.). The constructed plasmid was transformed into either electrocompetent or chemically competent DH5α λpir *E. coli*. The entire *binK* gene on the plasmid construct was sequenced (using pEVS107 F and R primers and *binK* sequencing primers). BinK alleles generated in this manner were then introduced into *V. fischeri* by tetraparental mating by mixing the pEVS104-containing helper, pUX-BF13-containing transposase, pEVS107 mini-Tn*7* vector-containing donor, and the *V. fischeri* recipient (51). PCR verification by amplifying around the *att*Tn*7* site with primers Tn*7* site F and Tn*7* site R confirmed transposon insertion at the *att*Tn*7* site.

Wrinkled colony assays. Cultures were grown overnight, and 8-μl aliquots were spotted onto LBS plates or LBS-calcium (10 mM $CaCl_2$). Plates were incubated at 25°C or 28°C for 48 h and imaged using a Leica M60 stereomicroscope with Leica FireCam software. For assays done with the pM1422 reporter, plates were also imaged on a Zeiss Axio Zoom.V16 large-field fluorescent stereo microscope and analyzed with Zen Blue software.

BinK peptide antibody creation and purification. ProSci (Poway, CA) analyzed the sequence of BinK and chose the peptide SEYGEMIDLPHKRKDNLDIIK as an epitope for polyclonal antibody production. This peptide was synthesized by ProSci and used to inoculate rabbits. Serum was analyzed at specific checkpoints to assess antibody production. Final bleed serum was then purified in our laboratory using the Proteus Protein A Mini Purification Starter kit and yielded approximately 1 mg/ml of the antibody. Purified antibody was diluted 1:1 in 50% glycerol, aliquoted into small volumes, and stored at −20°C. Single aliquots were thawed and used for each blot.

SDS-PAGE and Western blots. Overnight culture (1 ml) was pelleted, washed, and lysed in 1% SDS. The volume of SDS used to lyse the sample was adjusted based on the optical density at 600 nm (OD_{600}) of the overnight culture to standardize the concentration of total protein in the samples. The solution was then pelleted to remove cell debris, and the supernatant was mixed 1:1 with 2× Laemli sample buffer (Bio-Rad) and beta-mercaptoethanol. Samples were heated at 95°C for 15 min and loaded onto a 10% Bio-Rad Mini-Protean TGX precast gel. The gel was then transferred to a polyvinylidene difluoride (PVDF) membrane and blocked overnight in 5% nonfat milk. The purified anti-BinK-peptide antibody was used as the primary antibody in a 1:100 dilution in 0.5% nonfat milk in 1× Tris-buffered saline (TBS)-Tween 20. The secondary antibody was a 1:5,000 dilution of the Pierce goat anti-rabbit IgG (H+L)-horseradish peroxidase (HRP) conjugate (lot UK293475). Washes were done in 1× TBS-Tween 20. Blots were developed using the Thermo Scientific SuperSignal West Dura extended duration substrate and analyzed using a Licor Odyssey Fc machine.

Construction of *sypG*(D53E). Site-directed mutation of *sypG* was done using an allelic exchange approach modified from the laboratory's gene deletion protocol (https://doi.org/10.5281/zenodo.1470836). In brief, approximately 1.6 kb upstream sequence and 1.6 kb downstream sequence of the desired point mutation site in *sypG* were amplified from ES114 genomic DNA using primers designed

TABLE 1 Strains used in this study

Strain	Genotype	Source or reference(s)
V. fischeri		
MJM1100 = ES114	Natural isolate, squid light organ	56, 57
MJM1107	MJM1100 pVSV102	23
MJM1198	MJM1100 *rscS**	32
MJM1438	MJM1100 pM1422	J. F. Brooks II
MJM1538	MJM1100 pLostfoX-Kan	23
MJM1575	MJM1100 pVSV103	22
MJM2251	MJM1100 Δ*binK*	22
MJM2252	MJM2251 pLostfoX-Kan	22
MJM2255	MJM1100 *rscS** Δ*binK*	22
MJM2265	MJM2251 pVSV102	22
MJM2475	MJM1198 *att*Tn*7*::*binK*	22
MJM2476	MJM2255 *att*Tn*7*::*binK*	22
MJM2479	MJM1198 *att*Tn*7*::*erm*	22
MJM2480	MJM2255 *att*Tn*7*::*erm*	22
MJM2484	MJM2255 *att*Tn*7*::*binK*(H362Q)	J. F. Brooks II
MJM2493	MJM2251 pM1422	J. F. Brooks II
MJM2536 = KV3299	ES114 Δ*sypE sypF**	18, 42
MJM3210	MJM1198 *att*Tn*7*::*binK*(H362Q)	This study
MJM3213	MJM1198 *att*Tn*7*::*binK*(D794A)	This study
MJM3215	MJM2255 *att*Tn*7*::*binK*(D794A)	This study
MJM3218	MJM1198 *att*Tn*7*::*binK*(H362Q, D794A)	This study
MJM3220	MJM2255 *att*Tn*7*::*binK*(H362Q, D794A)	This study
MJM3221	MJM2251 pVSV103	This study
MJM3236	MJM2536 *sypG*(D53E)	This study
MJM3251	MJM1198 *att*Tn*7*::*binK*(D794E)	This study
MJM3252	MJM2255 *att*Tn*7*::*binK*(D794E)	This study
MJM3256	MJM1198 *att*Tn*7*::*binK*(E366A)	This study
MJM3257	MJM2255 Δ*binK att*Tn*7*::*binK*(E363A)	This study
MJM3775	MJM1100 Δ*rscS*::*erm-bar*	This study
MJM3903	MJM1100 Δ*rscS*::*bar*	This study
MJM4017	MJM1100 Δ*binK* Δ*rscS*::*erm-bar*	This study
MJM4018	MJM1100 Δ*binK* Δ*rscS*::*bar*	This study
MJM4071	MJM4018 pVSV102	This study
MJM4240	MJM3236 pVSV104	This study
MJM4241	MJM3236 pBinK	This study
MJM4242	KV3299 pVSV104	This study
MJM4243	KV3299 pBinK	This study
MJM4251	MJM1198 *att*Tn*7*::*binK*(H362Q, D794E)	This study
MJM4252	MJM2255 *att*Tn*7*::*binK*(H362Q, D794E)	This study
MJM4253	MJM1198 *att*Tn*7*::*binK*(T366Q)	This study
MJM4254	MJM2255 Δ*binK att*Tn*7*::*binK*(T366Q)	This study
MJM4255	MJM1198 *att*Tn*7*::*binK*(T366A)	This study
MJM4256	MJM2255 Δ*binK att*Tn*7*::*binK*(T366A)	This study
MJM4257	MJM3903 pM1422	This study
MJM4258	MJM4018 pM1422	This study
E. coli		
MJM534	CC118 λpir/pEVS104	51
MJM537	DH5α λpir	Laboratory stock
MJM542	DH5α λpir/pVSV102	58
MJM570	DH5α/pEVS79	51
MJM580	DH5α λpir/pVSV104	58
MJM637	S17-1 λpir/pUX-BF13	59
MJM658	DH5α λpir/pEVS107	60
MJM1422	DH5α λpir/pM1422	22
MJM2090	DH5α λpir/pLostfoX-Kan	23
MJM2384	DH5α λpir/pBinK	22
MJM2474	DH5α λpir/pTn7BinK	22
MJM2482	DH5α λpir/pTn7BinK(H362Q)	J. F. Brooks II
MJM3211	DH5α λpir/pDAT01	This study
MJM3216	DH5α λpir/pDAT02	This study
MJM3234	DH5α λpir/pDAT05	This study

(Continued on next page)

TABLE 1 (Continued)

Strain	Genotype	Source or reference(s)
MJM3241	DH5α λpir/pDAT10	This study
MJM3255	DH5α λpir/pDAT12	This study
MJM3478	π3813/pKV496	50
MJM4248	DH5α λpir/pDAT13	This study
MJM4249	DH5α λpir/pDAT14	This study
MJM4250	DH5α λpir/pDAT15	This study

using the NEB site-directed mutagenesis approach. These two fragments were then cloned into pEVS79 (which had been linearized by primers MRH001 and MRH002) using isothermal assembly (NEBuilder HiFi DNA assembly cloning kit) with the primer combinations listed in Table 3. The reaction was transformed into *E. coli* with selection for transformants on LB-chloramphenicol. PCR around the insertion using primers M13 For (−41) and M13 Rev (−48) was used to confirm plasmid candidates. The resulting candidates were then confirmed by sequencing and conjugated into the *V. fischeri* recipient (KV3299/MJM2536) by triparental mating with helper plasmid pEVS104, selecting for the chloramphenicol resistance of the plasmid backbone. Single recombinants in *V. fischeri* were screened for maintaining chloramphenicol resistance. To obtain double recombinants, single recombinants were then grown without antibiotics and patched onto LBS and LBS-Cam to find isolates that lost the antibiotic resistance cassette. These candidates were then verified with PCR and sequencing to confirm loss of the *cam* cassette and mutation of *sypG* to *sypG*(D53E). Strain MJM2536 *sypG*(D53E) was saved as MJM3236.

Construction of Δ*rscS* and Δ*binK* Δ*rscS* strains. Deletion of *rscS* was performed following the barcode-tagged gene deletion protocol from Burgos et al. (52). In brief, the upstream homology arm was amplified using primers KMB_082 and KMB_083 and the downstream homology arm was amplified using primers KMB_086 and KMB_087. Homology arms were fused to either side of a third fragment containing an *erm* cassette using splicing by overhang extension PCR (SOE PCR). Mutagenic DNA was purified using the Qiagen PCR purification kit and transformed into ES114 via transformation using pLostfoX-Kan (MJM1538) (53, 54). Mutant candidates were selected using erythromycin and screened by PCR using primer pairs KMB_081/KMB_088, KMB_081/HB8, and KMB_084/KMB_085. Insertion of the *erm-bar* scar was confirmed by Sanger sequencing using primers KMB_081, KMB_082, KMB_083, HB8, HB9, KMB_086, KMB_087, KMB_088, and the barcode sequence was recorded. The final bar code scar strain (MJM3903) was constructed via a triparental mating with donor MJM3478 (π3813/pKV496) (50) and helper strain MJM534 (CC118 λpir/pEVS104) with MJM3775. Candidates were selected for using kanamycin and screened by PCR using the primer pairs listed above. The deletion scar was verified by Sanger sequencing using primers KMB_081, KMB_082, KMB_083, HB41, HB42, KMB_086, KMB_087, and KMB_088.

To create the Δ*binK* Δ*rscS* strain, a Δ*binK* strain with the pLostfoX-Kan plasmid (MJM2252) was cultured for transformation (54). Donor DNA was 2.4 μg of genomic DNA from the Δ*rscS*::*erm-bar* strain that

TABLE 2 Plasmid list

Plasmid	Description[a]	Source or reference
pEVS107	Mini-Tn*7* mobilizable vector (Kan^r Erm^r)	60
pTn7BinK	pEVS107 carrying wild-type *binK* (Kan^r Erm^r)	22
pTn7BinK(H362Q)	pEVS107 encoding BinK H362Q mutant (Kan^r Erm^r)	This study
pDAT01	pEVS107 encoding BinK D794A mutant (Kan^r Erm^r)	This study
pDAT02	pEVS107 encoding BinK H362Q, D794A mutant (Kan^r Erm^r)	This study
pDAT10	pEVS107 encoding BinK D794E mutant (Kan^r Erm^r)	This study
pDAT13	pEVS107 encoding BinK H362Q, D794E mutant (Kan^r Erm^r)	This study
pDAT12	pEVS107 encoding BinK E363A mutant (Kan^r Erm^r)	This study
pDAT14	pEVS107 encoding BinK T366Q mutant (Kan^r Erm^r)	This study
pDAT15	pEVS107 encoding BinK T366A mutant (Kan^r Erm^r)	This study
pEVS104	Conjugal helper plasmid (Kan^r)	51
pUX-BF13	Tn*7* transposition helper (Amp^r)	59
pVSV104	Vector backbone for complementation (Kan^r)	58
pBinK	pVSV104 carrying wild-type *binK* (Kan^r)	22
pEVS79	Vector backbone for allelic exchange (Cam^r)	51
pDAT05	pEVS79 carrying *sypG* with D53E mutation (Cam^r)	This study
pM1422	pTM267 *sypA′-gfp*$^+$ (Cam^r)	22
pVSV102	Constitutive GFP (Kan^r)	58
pVSV103	Constitutive LacZ (Kan^r)	58
pLostfoX-Kan	Arabinose-inducible TfoX for transformation (Kan^r)	23
pKV496	pEVS79 containing the FLP recombinase (Kan^r)	50

[a]Kan, kanamycin; Amp, ampicillin; Cam, chloramphenicol; Erm, erythromycin; ^{r}, resistant; GFP, green fluorescent protein.

TABLE 3 Primer list

Primer name	Sequence (5′–3′)	Notes
DAT_011F BinK ext	CTTATGGGATAGCTTTAGCTCGAA	External primer to sequence around *binK* gene
DAT_012R BinK ext	TTCTTTATTAAGTGAAGGCGAACC	External primer to sequence around b*inK* gene
DAT_018F tfox	TAAATAAATCCTGGTGTCCCTGTT	Screen for pLostfoX-Kan
DAT_019R tfox	TCGCTGTTAAAAGGACAATTACAA	Screen for pLostfoX-Kan
DAT_064 D794A F	AGTTTTAATGGcgTGTATGATGCCGATAATG	Site-directed mutagenesis to make *binK*(D794A); lowercase letters represent mutated nucleotides
DAT_065 D794A R	AAACTATAAGGTGACGTTTTAC	Site-directed mutagenesis to make *binK*(D794A)
DAT_066 D794A Fwd	GAATCGTCCAAAAATTTGTTCCGC	Screen for D794A mutants
DAT_067 D794A RevM	CATCCATTATCGGCATCATACAcg	Screen for D794A mutants; lowercase letters represent nucleotides specific to mutant
DAT_068 D794A RevWT	CATCCATTATCGGCATCATACAgt	Screen for D794A mutants; lowercase letters represent nucleotides specific to the wild-type
DAT_071 sypG_US F	ccggtcgacggtatcgataaGATATTCTCGACTTCTCACGTATG	*sypG*-D53E cloning; capital letters indicate homology to template
DAT_072 sypG_US R	tcgagaatcaccaaatgTGGTGGATTCTTTTCCATAAATGC	*sypG*-D53E cloning; capital letters indicate homology to template
DAT_074 sypG_DS R	gcaggaattcgatatcaagcCTGGAATATAATGCCGCTTTGTAG	*sypG*-D53E cloning; capital letters indicate homology to template
DAT_077 sypG_DS F	CATTTGGTGATTCTCGAaTTGAAACTGCC	*sypG*-D53E cloning; lowercase letter represents mutated nucleotide
DAT_078 sypG seq1	CATGAAGGTTCTGGTTTAGGG	pEVS79 *sypG*-D53E sequencing
DAT_079 sypG seq2	CCGCTCTCTATCTGATAC	pEVS79 *sypG*-D53E sequencing
DAT_080 sypG seq3	GCATTAGAGTTTGAAGCG	pEVS79 *sypG*-D53E sequencing
DAT_081 sypG seq4	GATATGTCAGGGCAGGATG	pEVS79 *sypG*-D53E sequencing
DAT_082 sypG seq5	GTAAACGCAGCAATAAACC	pEVS79 *sypG*-D53E sequencing
DAT_083 sypG seq6	CGCAAAAGAAGATCATAA	pEVS79 *sypG*-D53E sequencing
DAT_084 sypG seq7	GATGGTAATGTTCTTAATG	pEVS79 *sypG*-D53E sequencing
DAT_085 sypG seq8	CCATTGGGCGAATTACAC	pEVS79 *sypG*-D53E sequencing
DAT_086 sypG seq9	GAATAGGCACAACATGGAC	pEVS79 *sypG*-D53E sequencing
DAT_087 sypG seq10	CCTGTACCGCTTTCACCA	pEVS79 *sypG*-D53E sequencing
DAT_088 sypG seq11	CATAAATGCCTTCGCTTG	pEVS79 *sypG*-D53E sequencing
DAT_089 sypG seq12	GATGGTTTCTACTCGCTC	pEVS79 *sypG*-D53E sequencing
DAT_090 sypG seq13	CATCCATTTCAGGCATAG	pEVS79 *sypG*-D53E sequencing
DAT_091 sypG seq14	GCTGTTATCTGCCATAGT	pEVS79 *sypG*-D53E sequencing
DAT_092 D53E Fwd	GAGTTTAATGAATCAACAGAAGAGC	*sypG*-D53E screen
DAT_093 D53E RevMT	CCCTGACATATCTGGCAGTTTCAAt	*sypG*-D53E screen; lowercase letter represents nucleotide specific to mutant
DAT_094 D53E RevWT	CCCTGACATATCTGGCAGTTTCAAa	*sypG*-D53E screen; lowercase letters represent nucleotide specific to the wild type
DAT_095 sypG fwd	CTACAGCAAGCCAGAAATGAAGCAG	Amplify around *sypG* insert area on pEVS79
DAT_096 sypG rev	GGGTGCCTTTTGATTGAATTAAGTTC	Amplify around *sypG* insert area on pEVS79
DAT_106 D794E F	TTTTAATGGAgTGTATGATGCC	Site-directed mutagenesis to make *binK*(D794E); lowercase letter represents mutated nucleotide
DAT_107 D794E R	CTAAACTATAAGGTGACGTTTTAC	Site-directed mutagenesis to make *binK*(D794E)
DAT_109 E363A_F	ATGTCACACGctATTCGAACAC	Site-directed mutagenesis to make *binK*(E363A); lowercase letters represent mutated nucleotides
DAT_110 E363_R	ATTAGCTAAAAATGAACTTTTGG	Site-directed mutagenesis to make *binK*(E363A)
DAT_111 T366A_F	CGAAATTCGAgcACCTCTAAATG	Site-directed mutagenesis to make *binK*(T366A); lowercase letters represent mutated nucleotides
DAT_112 T366_R	TGTGACATATTAGCTAAAAATG	Site-directed mutagenesis to make *binK* T366 mutants
DAT_114 T366Q_F	CGAAATTCGAcaACCTCTAAATGGCATC	Site-directed mutagenesis to make *binK*(T366Q); lowercase letters represent mutated nucleotides
DAT_118 D794E_RevWT	CATCCATTATCGGCATCATACAg	Screen for D794E mutants, lowercase letter represents nucleotide specific to the wild type
DAT_119 D794E_RevM	CATCCATTATCGGCATCATACAc	Screen for D794E mutants; lowercase letter represents nucleotide specific to mutant
DAT_120 E363A_RevM	CCATTTAGAGGTGTTCGAATag	Screen for E363A mutants; lowercase letters represent nucleotides specific to mutant
DAT_121 E363A_RevWT	CCATTTAGAGGTGTTCGAATtt	Screen for E363A mutants; lowercase letters represent nucleotides specific to the wild type
DAT_122 E363A_Fwd	GGTTGATCGGTGTTATTGAATC	Screen for E363A mutants

(Continued on next page)

TABLE 3 (Continued)

Primer name	Sequence (5′–3′)	Notes
DAT_257 T336 RevWT	CATACCAATGATGCCATTTAGAGGTgt	Screen for T366 mutants; lowercase letters represent nucleotides specific to the wild type
DAT_259 T366 RevQ	CATACCAATGATGCCATTTAGAGGTtg	Screen for T366 mutants; lowercase letters represent nucleotides specific to the T366Q mutant
DAT_260 T366 RevA	CATACCAATGATGCCATTTAGAGGTgc	Screen for T366 mutants; the lowercase letters represent nucleotides specific to the T366A mutant
DAT_261 T366 Fwd	CGCTGTTGATGAAAGTATGTATGTTGTAG	Screen for T366 mutants
Tn*7* site F	TGTTGATGATACCATTGAAGCTAAA	Amplify around *att*Tn*7* site
Tn*7* site R	CTTGCTGTATGTATTTGCTGATGA	Amplify around *att*Tn*7* site
pEVS107 F	ACCTATCAAGGTGTACTGCCTTCC	Sequences around pEVS107 multiple cloning site
pEVS107 R	GTCGTTAAATGCCCTTTACCTGT	Sequences around pEVS107 multiple cloning site
MRH001	TTATCGATACCGTCGACC	Linearizes pEVS79 for cloning
MRH002	GCTTGATATCGAATTCCTG	Linearizes pEVS79 for cloning
M13 Rev (−48)	AGCGGATAACAATTTCACACAGG	Amplifies around plasmid insertions
M13 For (−41)	CGCCAGGGTTTTCCCAGTCACGAC	Amplifies around plasmid insertions
JFB_359	AAATGATAATCGCTGGTC	Sequencing of *binK*
JFB_361	GATGTTCATCAAGCATTA	Sequencing of *binK*
JFB_362	GAGGTGTTCGAATTTCGT	Sequencing of *binK*
JFB_363	GAGCGAAAGTCTCATCAG	Sequencing of *binK*
JFB_364	AAACCTCAGACCATGAAA	Sequencing of *binK*
JFB_365	GGAAAGAGAATGATTAAG	Sequencing of *binK*
JFB_366	ATTCAAAGAATATGGTGC	Sequencing of *binK*
JFB_371	CTATTTTATTGGCTTGTG	Sequencing of *binK*
JFB_372	AACTGAAACCGATTTAAC	Sequencing of *binK*
JFB_373	ATGCCGTTAAATTTACTC	Sequencing of *binK*
JFB_374	TTGAGGTGATTGAGCCAA	Sequencing of *binK*
JFB_375	TTGAACGTACAATTGAAG	Sequencing of *binK*
JFB_376	TAGATATGGTGATGAGTA	Sequencing of *binK*
JFB_377	ACTGAATTACGTTTAACG	Sequencing of *binK*
JFB_426	GCTAATATGTCACAAGAAATTCGAACACC	Site-directed mutagenesis to make pTn7BinK (H362Q)
JFB_427	GGTGTTCGAATTTCTTGTGACATATTAGC	Site-directed mutagenesis to make pTn7BinK (H362Q)
KMB_081	GTGTGATGCAGATATAAAAAATCCCTGATCTTAATC	F0 for ES114 *rscS* deletion
KMB_082	CGAACTTCCCCACCAGCTAAAATC	F1 for ES114 *rscS* deletion
KMB_083	CTGGCGAAGCATATATAAGAAGCTCGTCTCGTCATTGCAT TAGCTCCTATAAAATAGTCTGTTTGG	R1-LL for ES114 *rscS* deletion
KMB_084	CACTACATTGCCGTAGAAAGAGACATCAC	FW for ES114 *rscS* deletion
KMB_085	CAGCTTGTTTACCTTTACCTGTTAGAGTATGG	RW for ES114 *rscS* deletion
KMB_086	GACTTGACCTGGATGTCTCTACCCACAAGATCGGAGAAGT ATGAAACACAATAAACTTCGTCATAAAAAAAGG	F2-RL for ES114 *rscS* deletion
KMB_087	CGTACTATGGTGTTTAATATCAATACACTTCAATGGG	R2 for ES114 *rscS* deletion
KMB_088	CTCTCGTGCTGTCATTCTTGACCAC	R0 for ES114 *rscS* deletion
HB8	ACAAAATTTTAAGATACTGCACTATCAACACACTCTTAAG	Sequencing of ES114 Δ*rscS*
HB9	GGGAGGAAATAATCTAGAATGCGAGAGTAGG	Sequencing of ES114 Δ*rscS*
HB41	CGATCTTGTGGGTAGAGACATCCAGGTCAAGTCCAGCCCC GCTCTAGTTTGGGAATCAAGTGCATGAGCGCTGAAG	Sequencing of ES114 Δ*rscS*
HB42	ACGAGACGAGCTTCTTATATATGCTTCGCCAG	Sequencing of ES114 Δ*rscS*

was purified using the Qiagen DNeasy Blood & Tissue kit. Transformed cells were plated onto LBS containing erythromycin to select for transformants. Isolates were then patched onto LBS containing kanamycin to ensure loss of the pLostfoX-Kan plasmid. PCR was performed to ensure that the strain was transformed with Δ*rscS*::*erm-bar* and maintained Δ*binK* (primers DAT_011F BinK ext, DAT_012R BinK ext, KMB_081, and KMB_088). The *erm* cassette was then removed using an FLP recombinase as described with the Δ*rscS*::*bar* strain above to create the final Δ*binK* Δ*rscS*::*bar* strain (MJM4018).

Squid single-strain colonizations. *V. fischeri* strains were grown overnight with aeration at 25°C in LBS. Overnight cultures were diluted 1:80 in LBS and grown to an OD_{600} of approximately 0.3. The OD_{600} was used to normalize the amount of each strain used to inoculate *E. scolopes* hatchlings at concentrations of approximately 6×10^3 CFU/ml in 40 ml seawater for 3 h. Squid were then washed and transferred to individual vials with 4 ml of bacterium-free filter-sterilized Instant Ocean (FSIO) until approximately 48 h postinoculation (hpi) with a water change that occurred at 24 hpi. At 48 hpi, squid were transferred to 1.5-ml microcentrifuge tubes with 750 ml of water, and each animal's luminescence was measured using the Promega GloMax 20/20 luminometer.

CFU counts per light organ were conducted as we described previously; euthanized squid were homogenized and plated, and colonies were counted to determine CFU per light organ (55).

For crypt visualization, squid were anesthetized in FSIO with 2% ethanol. At this point, hatchlings were either immediately dissected and imaged or fixed in 4% paraformaldehyde in 1× marine phosphate-buffered saline (mPBS; 50 mM phosphate buffer and 0.45 M NaCl [pH 7.4]) for approximately 36 h. Fixed squid were thoroughly washed in 1× mPBS before being dissected and imaged. All images were acquired on the Zeiss Axio Zoom.V16 large-field stereo microscope. The Zen Blue software polygon tool was used to select regions of interest and measure fluorescence intensity.

Squid aggregation assays. *V. fischeri* strains were grown overnight with aeration at 25°C in LBS. A 40-ml aliquot of overnight culture was used to inoculate *E. scolopes* hatchlings at concentrations of approximately 5.5×10^6 CFU/ml in 40 ml for 3 to 4 h. Hatchlings were then anesthetized in FSIO with 2% ethanol. At this point, hatchlings were either immediately dissected and imaged, or fixed in 4% paraformaldehyde in 1× mPBS (50 mM phosphate buffer and 0.45 M NaCl [pH 7.4]) for approximately 36 h. Fixed squid were thoroughly washed in 1× mPBS before being dissected and imaged. All images were acquired on the Zeiss Axio Zoom.V16 large-field fluorescent stereo microscope. The Zen Blue software polygon tool was used to select regions of interest and measure both area and fluorescence intensity.

Squid competition assays. Strains were grown overnight with aeration at 25°C in LBS and LBS containing kanamycin to maintain plasmid pVSV103. Strains with pVSV103 constitutively express LacZ (β-galactosidase). Overnight cultures were diluted 1:80 in LBS and grown to an OD_{600} of approximately 0.3. Using optical density to normalize the strains, the two strains were mixed in a 1:1 ratio. This mixed culture was used to inoculate *E. scolopes* hatchlings at concentrations of approximately 7.6×10^3 bacteria for 3 h. Squid were then washed and transferred to 40 ml of bacterium-free filter-sterilized Instant Ocean (FSIO) until approximately 48 h postinoculation (water was changed at 24 h postinoculation), at which point they were euthanized by storage at −80°C. Each squid was homogenized and plated on LBS–5-bromo-4-chloro-3-indolyl-β-D-galactopyranoside (X-Gal), and the blue/white colony ratios were used to score these competitions as described previously (23, 55).

Data analysis and graphing. Data analysis was conducted using Python, including the *pandas* library (62). For fluorescence of colonies, aggregates, and crypts, the mean GFP and mCherry values for the region of interest and a nearby background region were acquired using Zen Blue Software. The background for each channel was subtracted from the region of interest. To normalize GFP to plasmid copy number, the GFP reading was divided by the mCherry reading. This resulted in the reported mean GFP/mCherry reading for each individual colony, aggregate, or crypt space. GraphPad Prism was used to construct graphs and perform statistical analyses.

SUPPLEMENTAL MATERIAL

Supplemental material is available online only.

SUPPLEMENTAL FILE 1, PDF file, 2.6 MB.

ACKNOWLEDGMENTS

We thank John F. Brooks II for contributing strains for this study and Karen L. Visick for helpful comments on the manuscript.

This work was funded by NIGMS grant R35 GM119627 to M.J.M. Support for trainees was provided by NIGMS T32 GM008061 (D.A.L.), T32 GM008349 (K.M.B.), and an NSF Graduate Research Fellowship (K.M.B.).

REFERENCES

1. Ruby E, Henderson B, McFall-Ngai M. 2004. We get by with a little help from our (little) friends. Science 303:1305–1307. https://doi.org/10.1126/science.1094662.
2. McFall-Ngai MJ. 2014. The importance of microbes in animal development: lessons from the squid-*Vibrio* symbiosis. Annu Rev Microbiol 68:177–194. https://doi.org/10.1146/annurev-micro-091313-103654.
3. Nyholm SV, Stabb EV, Ruby EG, McFall-Ngai MJ. 2000. Establishment of an animal-bacterial association: recruiting symbiotic vibrios from the environment. Proc Natl Acad Sci U S A 97:10231–10235. https://doi.org/10.1073/pnas.97.18.10231.
4. Mandel MJ, Dunn AK. 2016. Impact and influence of the natural *Vibrio*-squid symbiosis in understanding bacterial-animal interactions. Front Microbiol 7:1982. https://doi.org/10.3389/fmicb.2016.01982.
5. Visick KL, Ruby EG. 2006. *Vibrio fischeri* and its host: it takes two to tango. Curr Opin Microbiol 9:632–638. https://doi.org/10.1016/j.mib.2006.10.001.
6. Ruby EG. 1996. Lessons from a cooperative, bacterial-animal association: the *Vibrio fischeri-Euprymna scolopes* light organ symbiosis. Annu Rev Microbiol 50:591–624. https://doi.org/10.1146/annurev.micro.50.1.591.
7. Ruby EG, McFall-Ngai MJ. 1992. A squid that glows in the night: development of an animal-bacterial mutualism. J Bacteriol 174:4865–4870. https://doi.org/10.1128/jb.174.15.4865-4870.1992.
8. Koch EJ, Miyashiro T, McFall-Ngai MJ, Ruby EG. 2014. Features governing symbiont persistence in the squid-vibrio association. Mol Ecol 23:1624–1634. https://doi.org/10.1111/mec.12474.
9. Nyholm SV, McFall-Ngai MJ. 2004. The winnowing: establishing the squid-*Vibrio* symbiosis. Nat Rev Microbiol 2:632–642. https://doi.org/10.1038/nrmicro957.
10. Yip ES, Geszvain K, DeLoney-Marino CR, Visick KL. 2006. The symbiosis regulator *rscS* controls the *syp* gene locus, biofilm formation and symbiotic aggregation by *Vibrio fischeri*. Mol Microbiol 62:1586–1600. https://doi.org/10.1111/j.1365-2958.2006.05475.x.
11. Yip ES, Grublesky BT, Hussa EA, Visick KL. 2005. A novel, conserved cluster of genes promotes symbiotic colonization and σ^{54}-dependent biofilm formation by *Vibrio fischeri*. Mol Microbiol 57:1485–1498. https://doi.org/10.1111/j.1365-2958.2005.04784.x.
12. Visick KL. 2009. An intricate network of regulators controls biofilm formation and colonization by *Vibrio fischeri*. Mol Microbiol 74:782–789. https://doi.org/10.1111/j.1365-2958.2009.06899.x.
13. Mandel MJ, Wollenberg MS, Stabb EV, Visick KL, Ruby EG. 2009. A single regulatory gene is sufficient to alter bacterial host range. Nature 458:215–218. https://doi.org/10.1038/nature07660.
14. Pankey SM, Foxall RL, Ster IM, Perry LA, Schuster BM, Donner RA, Coyle M, Cooper VS, Whistler CA. 2017. Host-selected mutations converging on a

global regulator drive an adaptive leap towards symbiosis in bacteria. Elife 6:e24414. https://doi.org/10.7554/eLife.24414.
15. Rotman ER, Bultman KM, Brooks JF, 2nd, Gyllborg MC, Burgos HL, Wollenberg MS, Mandel MJ. 2019. Natural strain variation reveals diverse biofilm regulation in squid-colonizing *Vibrio fischeri*. J Bacteriol 201: e00033-19. https://doi.org/10.1128/JB.00033-19.
16. Geszvain K, Visick KL. 2008. The hybrid sensor kinase RscS integrates positive and negative signals to modulate biofilm formation in *Vibrio fischeri*. J Bacteriol 190:4437–4446. https://doi.org/10.1128/JB.00055-08.
17. Norsworthy AN, Visick KL. 2015. Signaling between two interacting sensor kinases promotes biofilms and colonization by a bacterial symbiont. Mol Microbiol 96:233–248. https://doi.org/10.1111/mmi.12932.
18. Hussa EA, Darnell CL, Visick KL. 2008. RscS functions upstream of SypG to control the *syp* locus and biofilm formation in *Vibrio fischeri*. J Bacteriol 190:4576–4583. https://doi.org/10.1128/JB.00130-08.
19. Darnell CL, Hussa EA, Visick KL. 2008. The putative hybrid sensor kinase SypF coordinates biofilm formation in *Vibrio fischeri* by acting upstream of two response regulators, SypG and VpsR. J Bacteriol 190:4941–4950. https://doi.org/10.1128/JB.00197-08.
20. Ray VA, Eddy JL, Hussa EA, Misale M, Visick KL. 2013. The *syp* enhancer sequence plays a key role in transcriptional activation by the σ^{54}-dependent response regulator SypG and in biofilm formation and host colonization by *Vibrio fischeri*. J Bacteriol 195:5402–5412. https://doi.org/10.1128/JB.00689-13.
21. Morris AR, Visick KL. 2013. The response regulator SypE controls biofilm formation and colonization through phosphorylation of the *syp*-encoded regulator SypA in *Vibrio fischeri*. Mol Microbiol 87:509–525. https://doi.org/10.1111/mmi.12109.
22. Brooks JF, 2nd, Mandel MJ. 2016. The histidine kinase BinK is a negative regulator of biofilm formation and squid colonization. J Bacteriol 198:2596–2607. https://doi.org/10.1128/JB.00037-16.
23. Brooks JF, 2nd, Gyllborg MC, Cronin DC, Quillin SJ, Mallama CA, Foxall R, Whistler C, Goodman AL, Mandel MJ. 2014. Global discovery of colonization determinants in the squid symbiont *Vibrio fischeri*. Proc Natl Acad Sci U S A 111:17284–17289. https://doi.org/10.1073/pnas.1415957111.
24. Tischler AH, Lie L, Thompson CM, Visick KL. 2018. Discovery of calcium as a biofilm-promoting signal for *Vibrio fischeri* reveals new phenotypes and underlying regulatory complexity. J Bacteriol 200:e00016-18. https://doi.org/10.1128/JB.00016-18.
25. Thompson CM, Tischler AH, Tarnowski DA, Mandel MJ, Visick KL. 2019. Nitric oxide inhibits biofilm formation by *Vibrio fischeri* via the nitric oxide sensor HnoX. Mol Microbiol 111:187–203. https://doi.org/10.1111/mmi.14147.
26. Marchler-Bauer A, Bryant SH. 2004. CD-Search: protein domain annotations on the fly. Nucleic Acids Res 32:W327–W331. https://doi.org/10.1093/nar/gkh454.
27. Blum M, Chang H-Y, Chuguransky S, Grego T, Kandasaamy S, Mitchell A, Nuka G, Paysan-Lafosse T, Qureshi M, Raj S, Richardson L, Salazar GA, Williams L, Bork P, Bridge A, Gough J, Haft DH, Letunic I, Marchler-Bauer A, Mi H, Natale DA, Necci M, Orengo CA, Pandurangan AP, Rivoire C, Sigrist CJA, Sillitoe I, Thanki N, Thomas PD, Tosatto SCE, Wu CH, Bateman A, Finn RD. 2021. The InterPro protein families and domains database: 20 years on. Nucleic Acids Res 49:D344–D354. https://doi.org/10.1093/nar/gkaa977.
28. Letunic I, Khedkar S, Bork P. 2021. SMART: recent updates, new developments and status in 2020. Nucleic Acids Res 49:D458–D460. https://doi.org/10.1093/nar/gkaa937.
29. Mistry J, Chuguransky S, Williams L, Qureshi M, Salazar GA, Sonnhammer ELL, Tosatto SCE, Paladin L, Raj S, Richardson LJ, Finn RD, Bateman A. 2021. Pfam: the protein families database in 2021. Nucleic Acids Res 49: D412–D419. https://doi.org/10.1093/nar/gkaa913.
30. Wise AA, Fang F, Lin Y-H, He F, Lynn DG, Binns AN. 2010. The receiver domain of hybrid histidine kinase VirA: an enhancing factor for *vir* gene expression in *Agrobacterium tumefaciens*. J Bacteriol 192:1534–1542. https://doi.org/10.1128/JB.01007-09.
31. Wise AA, Binns AN. 2015. The receiver of the *Agrobacterium tumefaciens* VirA histidine kinase forms a stable interaction with VirG to activate virulence gene expression. Front Microbiol 6:1546. https://doi.org/10.3389/fmicb.2015.01546.
32. Singh P, Brooks JF, 2nd, Ray VA, Mandel MJ, Visick KL. 2015. CysK plays a role in biofilm formation and colonization by *Vibrio fischeri*. Appl Environ Microbiol 81:5223–5234. https://doi.org/10.1128/AEM.00157-15.
33. Freeman JA, Lilley BN, Bassler BL. 2000. A genetic analysis of the functions of LuxN: a two-component hybrid sensor kinase that regulates quorum sensing in *Vibrio harveyi*. Mol Microbiol 35:139–149. https://doi.org/10.1046/j.1365-2958.2000.01684.x.
34. Gao R, Stock AM. 2009. Biological insights from structures of two-component proteins. Annu Rev Microbiol 63:133–154. https://doi.org/10.1146/annurev.micro.091208.073214.
35. Bhate MP, Molnar KS, Goulian M, DeGrado WF. 2015. Signal transduction in histidine kinases: insights from new structures. Structure 23:981–994. https://doi.org/10.1016/j.str.2015.04.002.
36. Atkinson MR, Ninfa AJ. 1993. Mutational analysis of the bacterial signal-transducing protein kinase/phosphatase nitrogen regulator II (NRII or NtrB). J Bacteriol 175:7016–7023. https://doi.org/10.1128/jb.175.21.7016-7023.1993.
37. Willett JW, Kirby JR. 2012. Genetic and biochemical dissection of a HisKA domain identifies residues required exclusively for kinase and phosphatase activities. PLoS Genet 8:e1003084. https://doi.org/10.1371/journal.pgen.1003084.
38. Huynh TN, Noriega CE, Stewart V. 2010. Conserved mechanism for sensor phosphatase control of two-component signaling revealed in the nitrate sensor NarX. Proc Natl Acad Sci U S A 107:21140–21145. https://doi.org/10.1073/pnas.1013081107.
39. Huynh TN, Stewart V. 2011. Negative control in two-component signal transduction by transmitter phosphatase activity. Mol Microbiol 82:275–286. https://doi.org/10.1111/j.1365-2958.2011.07829.x.
40. Dutta R, Yoshida T, Inouye M. 2000. The critical role of the conserved Thr247 residue in the functioning of the osmosensor EnvZ, a histidine kinase/phosphatase, in *Escherichia coli*. J Biol Chem 275:38645–38653. https://doi.org/10.1074/jbc.M005872200.
41. Wayne KJ, Li S, Kazmierczak KM, Tsui H-CT, Winkler ME. 2012. Involvement of WalK (VicK) phosphatase activity in setting WalR (VicR) response regulator phosphorylation level and limiting cross-talk in *Streptococcus pneumoniae* D39 cells. Mol Microbiol 86:645–660. https://doi.org/10.1111/mmi.12006.
42. Thompson CM, Marsden AE, Tischler AH, Koo J, Visick KL. 2018. *Vibrio fischeri* biofilm formation prevented by a trio of regulators. Appl Environ Microbiol 84:e01257-18. https://doi.org/10.1128/AEM.01257-18.
43. Visick KL, Skoufos LM. 2001. Two-component sensor required for normal symbiotic colonization of *Euprymna scolopes* by *Vibrio fischeri*. J Bacteriol 183:835–842. https://doi.org/10.1128/JB.183.3.835-842.2001.
44. Kinoshita-Kikuta E, Kinoshita E, Eguchi Y, Koike T. 2016. Validation of *cis* and *trans* modes in multistep phosphotransfer signaling of bacterial tripartite sensor kinases by using Phos-tag SDS-PAGE. PLoS One 11: e0148294. https://doi.org/10.1371/journal.pone.0148294.
45. Teran-Melo JL, Peña-Sandoval GR, Silva-Jimenez H, Rodriguez C, Alvarez AF, Georgellis D. 2018. Routes of phosphoryl group transfer during signal transmission and signal decay in the dimeric sensor histidine kinase ArcB. J Biol Chem 293:13214–13223. https://doi.org/10.1074/jbc.RA118.003910.
46. Jacob-Dubuisson F, Mechaly A, Betton J-M, Antoine R. 2018. Structural insights into the signalling mechanisms of two-component systems. Nat Rev Microbiol 16:585–593. https://doi.org/10.1038/s41579-018-0055-7.
47. Chang CH, Zhu J, Winans SC. 1996. Pleiotropic phenotypes caused by genetic ablation of the receiver module of the *Agrobacterium tumefaciens* VirA protein. J Bacteriol 178:4710–4716. https://doi.org/10.1128/jb.178.15.4710-4716.1996.
48. Altura MA, Heath-Heckman EAC, Gillette A, Kremer N, Krachler A-M, Brennan C, Ruby EG, Orth K, McFall-Ngai MJ. 2013. The first engagement of partners in the *Euprymna scolopes-Vibrio fischeri* symbiosis is a two-step process initiated by a few environmental symbiont cells. Environ Microbiol 15:2937–2950. https://doi.org/10.1111/1462-2920.12179.
49. Le Roux F, Binesse J, Saulnier D, Mazel D. 2007. Construction of a *Vibrio splendidus* mutant lacking the metalloprotease gene *vsm* by use of a novel counterselectable suicide vector. Appl Environ Microbiol 73:777–784. https://doi.org/10.1128/AEM.02147-06.
50. Visick KL, Hodge-Hanson KM, Tischler AH, Bennett AK, Mastrodomenico V. 2018. Tools for rapid genetic engineering of *Vibrio fischeri*. Appl Environ Microbiol 84:e00850-18. https://doi.org/10.1128/AEM.00850-18.
51. Stabb EV, Ruby EG. 2002. RP4-based plasmids for conjugation between *Escherichia coli* and members of the *Vibrionaceae*. Methods Enzymol 358:413–426. https://doi.org/10.1016/s0076-6879(02)58106-4.
52. Burgos HL, Burgos EF, Steinberger AJ, Suen G, Mandel MJ. 2020. Multiplexed competition in a synthetic squid light organ microbiome using barcode-tagged gene deletions. mSystems 5:e00846-20. https://doi.org/10.1128/mSystems.00846-20.
53. Brooks JF, 2nd, Gyllborg MC, Kocher AA, Markey LEH, Mandel MJ. 2015. TfoX-based genetic mapping identifies *Vibrio fischeri* strain-level differences and

reveals a common lineage of laboratory strains. J Bacteriol 197:1065–1074. https://doi.org/10.1128/JB.02347-14.
54. Pollack-Berti A, Wollenberg MS, Ruby EG. 2010. Natural transformation of *Vibrio fischeri* requires *tfoX* and *tfoY*. Environ Microbiol 12:2302–2311.
55. Naughton LM, Mandel MJ. 2012. Colonization of *Euprymna scolopes* squid by *Vibrio fischeri*. J Vis Exp (61):e3758. https://doi.org/10.3791/3758.
56. Boettcher KJ, Ruby EG. 1990. Depressed light emission by symbiotic *Vibrio fischeri* of the sepiolid squid *Euprymna scolopes*. J Bacteriol 172:3701–3706. https://doi.org/10.1128/jb.172.7.3701-3706.1990.
57. Mandel MJ, Stabb EV, Ruby EG. 2008. Comparative genomics-based investigation of resequencing targets in *Vibrio fischeri*: focus on point miscalls and artefactual expansions. BMC Genomics 9:138. https://doi.org/10.1186/1471-2164-9-138.
58. Dunn AK, Millikan DS, Adin DM, Bose JL, Stabb EV. 2006. New *rfp*- and pES213-derived tools for analyzing symbiotic *Vibrio fischeri* reveal patterns of infection and *lux* expression *in situ*. Appl Environ Microbiol 72:802–810. https://doi.org/10.1128/AEM.72.1.802-810.2006.
59. Bao Y, Lies DP, Fu H, Roberts GP. 1991. An improved Tn*7*-based system for the single-copy insertion of cloned genes into chromosomes of gram-negative bacteria. Gene 109:167–168. https://doi.org/10.1016/0378-1119(91)90604-A.
60. McCann J, Stabb EV, Millikan DS, Ruby EG. 2003. Population dynamics of *Vibrio fischeri* during infection of *Euprymna scolopes*. Appl Environ Microbiol 69:5928–5934. https://doi.org/10.1128/aem.69.10.5928-5934.2003.
61. Madeira F, Park YM, Lee J, Buso N, Gur T, Madhusoodanan N, Basutkar P, Tivey ARN, Potter SC, Finn RD, Lopez R. 2019. The EMBL-EBI search and sequence analysis tools APIs in 2019. Nucleic Acids Res 47:W636–W641. https://doi.org/10.1093/nar/gkz268.
62. The pandas development team. 2021. pandas-dev/pandas: Pandas. Zenodo. https://doi.org/10.5281/zenodo.3509134.